Available online at www.sciencedirect.com
SCIENCE DIRECT®
International Journal of Heat and Mass Transfer 47 (2004) 2735–2745
International Journal of HEAT and MASS TRANSFER
www.elsevier.com/locate/ijhmt

A one-dimensional thermo-fluid model of blood circulation in the human upper limb

Ying He [a,*], Hao Liu [b], Ryutaro Himeno [a]

[a] Computational Biomechanics Unit, RIKEN, 2-1 Hirosawa, Wako-shi, Saitama 351-0198, Japan
[b] Department of Electronics and Mechanical Engineering, Faculty of Engineering, Chiba University, 1-33 Yayoi-cho, Inage-ku, Chiba 263-8522, Japan

Received 17 January 2003; received in revised form 30 October 2003

Abstract

Blood circulation is considered to play an important role in heat transfer between living tissues, particularly, in peripheral vessels wherein the temperature is, generally, closely related with blood flow rate. The aim of this paper is to study the influence of blood flow rate on body temperature by means of a one-dimensional thermo-fluid model. This model has been recently developed for the circulation system of the upper limb and involves arteries, capillaries, and veins. Computed results of the blood flow, cross-sectional area, and temperature of each vessel are presented, and are then compared with available experimental data. The influence of the bending stiffness of the vessel walls as well as that of blood viscosity on blood pressure and temperature is analyzed.

Keywords: Blood flow; Numerical modeling; Blood circulation; Bioheat transfer; Tissue

1. Introduction

Human body temperature depends on the circulation system as well as the various aspects of its control mechanism. In addition to this, environmental temperature also affects the physiological functions of blood vessels and other organs. Therefore, a comprehensive study on the relationship between blood flow rate and body temperature is of great physiological significance. Several experimental studies point out that the flow rate in the peripheral vessels of the hand is closely related to fingertip temperature: e.g., haemodynamics change while smoking, and mental stress affects fingertip temperature [1,2]. It is also reported that there exists a difference in thermal regulation ability between men and women due to a difference in their ability to control the blood flow rate [3]. Additionally, aging may result in a decrease in thermoregulatory ability due to the variation in vessel wall properties and blood flow rate [4]. The one-dimensional fluid dynamic model in an elastic tube model of blood vessels is frequently applied to analyze blood pressure and flow waveform in arteries. Kitawaki et al. [5] proposed a one-dimensional model to investigate the effect of unsteady viscosity in a single tube, when the tube law was used to express the viscoelasticity of the arterial wall. The scheme (Jameson–Baker) has fourth-order accuracy in space and time. The simulated results were in agreement with the measurements when compared to the experimental results obtained using the silicone rubber tube. Although their work is of significance in investigating the viscoelasticity of arterial blood, the high-order accuracy scheme may limit its application to the computation of systemic blood circulation.

Many other models have also been proposed to analyze the pressure and flow waveforms for the circulation system of the entire human body from the viewpoint of clinical applications. Among them, the

* Corresponding author. Tel.: +81-48-467-4536; fax: +81-48-467-4532.
E-mail addresses: heying@riken.jp, heyingshao@hotmail.com (Y. He).

0017-9310/$ - see front matter © 2004 Elsevier Ltd. All rights reserved.
doi:10.1016/j.ijheatmasstransfer.2003.10.041

Nomenclature

A	cross-sectional area of blood vessel (m^2)
A_s	surface area of blood vessel per unit (m)
B, C	parameters defined in Eqs. (8) and (9)
c	specific heat (J/kg K)
E	Young's modulus (kg/s^2 m)
F	friction term defined in Eq. (10)
G, G_F	parameters defined in Eq. (19)
h	wall thickness of blood vessel (m)
h_{ves}	heat transfer coefficient (W/m^2 K)
k_p	proportional factor in Eq. (5) (Pa)
k_1, k_3	proportional parameters in Eq. (6) (kg/s^2 m)
k_2	proportional parameter in Eq. (6) (m^{-1})
L	length of blood vessel (m)
N	total number of vessels included in the equivalent blood vessel
p	pressure (Pa)
q	flow rate (m^3/s)
r	radius of blood vessel (m), r direction in cylindrical coordinate (m)
S	total cross-sectional area of the equivalent blood vessel (m^2)
T	temperature (K)
t	time (s)
u	velocity in x direction (m/s)
x	axial length coordinate (m)
δ	thickness of the boundary layer (m)
λ	thermal conductivity (W/m K)
v	kinematic viscosity (m^2/s)
θ	θ direction in cylindrical coordinate
ρ	density (kg/m^3)
ω	blood perfusion rate ($m^3/s/m^3$)
ψ	radial frequency (rad/s)
Δt	time increment (s)
Δx	spatial increment (m)

Subscripts

0	initial state, initial point in the daughter or east vessel
b	blood
bot	bottom
d1, d2	daughter vessels
e	east
in	parameter at inlet
i, j, k	spatial indices
m	the last point in the mother or west vessel
met	metabolic
p	parent vessel
t	tissue
top	top
tmn	mean tissue temperature at position x
w	west
r	r direction
θ	θ direction

Superscript

n, $n+1$	time step

structured-tree model of systemic arteries by Olufsen et al. [6] may be the latest one. They created a systemic artery tree based on magnetic resonance measurements and statistical relationships. The blood flow in the larger arteries is modeled by using the one-dimensional equations derived from the axisymmetric Navier–Stokes equations for flow in an elastic tube. For the blood flow in small arteries and arterioles, a linearized governing equation was introduced to calculate the root impedance of the structured arterial tree. The blood flow and pressure are computed as functions of time and axial distance within each of the arteries. The computed blood flow and pressure in each artery showed a satisfactory agreement with the magnetic resonance measurements.

On the other hand, various models have been developed to simulate the human blood circulation system (arteries, capillaries, and veins). For example, Zagzoule and Marc-Vergnes [7] presented a global mathematical model of cerebral circulation in humans. Li and Cheng [8] explored the global response of pulmonary circulation using a nonlinear model, and Sheng et al. [9] developed a computational model to investigate the behavior of the entire human systemic circulation. The distinguishing characteristic of their work is that they considered the entire circulation system in their models. However, they used the traditional mathematical governing equation wherein the axisymmetric and no-slip conditions were not considered. In this regard, Olufsen et al. [6] made an improvement in their study.

With respect to the mathematical model for bio-heat transfer, Keller and Seiler [10,11] have presented a model that considers the heat transfer among separate tissues, arteries, and venous parts, and they derived steady-state energy equations for the arteries, veins, and tissues. However, the variations in blood vessels are not considered.

Although the variations in blood flow, blood pressure, and temperature are investigated separately in the above models, the relationships between them are not studied. Craciunescu and Clegg [12] used the coupled Navier–Stokes and energy equations to investigate the effect of blood velocity pulsations on bio-heat transfer. Although they obtained important results regarding the relationship between the pulsating axial velocity and

temperature profile and the effect of the Womersley number variation, they did not consider the variations in the vessel tube and the global effect of blood flow.

In the authors' previous study [13], a two-dimensional, finite element thermo-fluid model was developed to investigate the effect of blood flow on the temperature distribution of a finger. The finger consists of counter-current major arterial and venous blood vessels, bone, tendon, and skin. We assumed that the blood vessels were rigid, and the basic Navier–Stokes equations and the energy equation were employed to describe the behavior of the blood flow and the solid tissues. The computed results showed that the skin temperature decreased with decreasing blood flow velocity. However, the degree of temperature variation with differing blood flow velocity was quite minimal, implying that the effect of the cross-sectional area of a blood vessel should be used in investigating the relationship between the blood flow rate and temperature in the peripheral circulation system. The development of a one-dimensional thermo-fluid model of a blood vessel that incorporates the effects of blood flow rate, transmural pressure, cross-sectional area, and elasticity of the blood vessel would, therefore, be valuable.

This paper presents a thermo-fluid model of blood circulation in the upper limb of humans. Not only are the blood flow rates and pressures in larger arteries considered, but the flow rates and pressures in arterioles, capillaries, and veins are also included. Based on the model by Olufsen et al. [6], the fluid dynamic model is developed, where the properties of the vessel wall in the arteries, microcirculation, and veins are assumed to vary in different ways. The energy equation in compliant vessels is developed based on Keller and Seiler's analytical method.

The two-step Lax-Wendroff method is employed in computing the flow rate and cross-sectional area, and the upwind scheme is used to transform the energy equation into an algebraic form. The blood pressure, flow rate, and temperature are obtained for different vessels. The blood pressure signals are in favorable agreement with available experimental data [14]. The predicted temperature shows a moderate changing tendency from arteries to veins. The influence of the bending stiffness of arteries as well as that of blood viscosity is also investigated.

2. Morphology of the blood circulation in the upper limb

Fig. 1 shows the schematic diagram of an arterial and venous system of the human upper limb. The circulation begins from the ascending aorta (No. 1). The bifurcations of the vessels are based on anatomic knowledge. Following the ascending aorta, are the anonyma artery, the subclavian artery, and the two ulnar arteries (The ulnar arteries are before and after the bifurcation of the

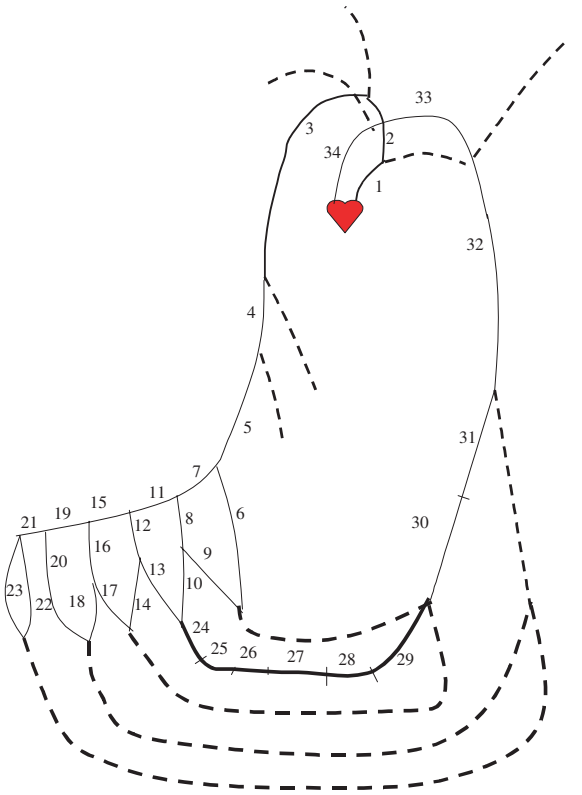

Fig. 1. A schematic diagram of the arterial and venous systems of the human upper limb.

interosseous artery), numbered as 2, 3, 4, and 5 respectively. There are many kinds of bifurcations in palmar arteries. Here, we assumed that the arteries in the palmar side have the same kind of bifurcation as the arteries in the dorsal side, and that they are formed only from the ulnar artery (Nos. 6–23). About 27% of the general population has this kind of structure [15].

The microcirculation includes terminal arteries, arterioles, capillaries, venules, terminal veins, and palmar veins (Nos. 24–29). In this component, each equivalent vessel is made up of a number of vessels having the same diameter and length.

The vessels of Nos. 30–34 represent the returning veins in the upper limb. They are the basilic vein, the brachial vein, the subclavian vein, the anonyma vein, and the superior vena cava, respectively.

The diameters and lengths of the vessels are defined on the basis of statistical data in previous studies [6,7,9,16], and the anatomic atlas [15]. The arterial vessels are assumed to taper exponentially along the axial direction [6], that is,

$$r_0(x) = r_{\text{top}} \exp\left(\log\left(\frac{r_{\text{bot}}}{r_{\text{top}}}\right)\frac{x}{L}\right). \quad (1)$$

Table 1
Physiological data of the arteries for the thermo-fluid model

Segment number	Vessels	Length (m)	Proximal radius (m)	Distal radius (m)	Number of vessels
1	Ascending aorta	0.07	1.25e−2	1.14e−2	1
2	Anonyma artery	0.035	0.7e−2	0.7e−2	1
3	Subclavian artery	0.43	0.44e−2	0.28e−2	1
4	Ulnar artery	0.067	0.215e−2	0.215e−2	1
5	Ulnar artery	0.171	0.203e−2	0.184e−2	1
6	Proper palmar digital artery	0.14	0.055e−2	0.045e−2	1
7	Superficial palmar arch	0.01	0.18e−2	0.18e−2	1
8	Common palmar digital artery	0.08	0.68e−2	0.68e−2	1
9	Proper palmar digital artery	0.08	0.05e−2	0.05e−2	1
10	Proper palmar digital artery	0.08	0.05e−2	0.05e−2	1
11	Superficial palmar arch	0.006	0.16e−2	0.16e−2	1
12	Common palmar digital artery	0.08	0.068e−2	0.068e−2	1
13	Proper palmar digital artery	0.08	0.05e−2	0.05e−2	1
14	Proper palmar digital artery	0.08	0.05e−2	0.05e−2	1
15	Superficial palmar arch	0.006	0.144e−2	0.144e−2	1
16	Common palmar digital artery	0.08	0.068e−2	0.068e−2	1
17	Proper palmar digital artery	0.08	0.05e−2	0.05e−2	1
18	Proper palmar digital artery	0.08	0.05e−2	0.05e−2	1
19	Common palmar digital artery	0.006	0.13e−2	0.13e−2	1
20	Proper palmar digital artery	0.15	0.06e−2	0.05e−2	1
21	Principal artery of thumb	0.02	0.1e−2	0.1e−2	1
22	Proper palmar digital artery	0.06	0.066e−2	0.066e−2	1
23	Proper palmar digital artery	0.06	0.066e−2	0.066e−2	1

Table 2
Physiological data of the capillaries and veins for the thermo-fluid model

Segment number	Vessels	Length (m)	Area (m^2)	Number of vessels
24	Terminal arteries	0.08	0.063e−4	32
25	Arterioles	0.018	0.75e−4	2.4e+5
26	Capillaries	0.002	7.5e−4	1.0e+6
27	Venules	0.02	2.55e−4	0.36e+6
28	Terminal veins	0.08	0.42e−4	36
29	Dorsal venous network of hand	0.08	0.43e−4	2
30	Ulnar veins	0.3	1e−4	2
31	Brachial vein	0.15	0.85e−4	1
32	Subclavian vein	0.2	0.9e−4	1
33	Anonyma vein	0.065	2.5e−4	1
34	Superior vena cava	0.045	4.5e−4	1

The diameters of capillaries and veins are assumed to be constant along the axial direction. The morphological data used in this model are listed in Tables 1 and 2.

3. Governing equations

Predicting the temperature of blood flowing in a compliant vessel requires four governing equations: two to ensure the conservation of mass and the conservation of momentum, one to obey the law of elasticity, and one to satisfy the conservation of energy. The continuity and momentum equations may be respectively defined as:

$$\frac{\partial A}{\partial t}+\frac{\partial q}{\partial x}=0, \tag{2}$$

$$\frac{\partial q}{\partial t}+\frac{\partial}{\partial x}\left(\frac{q^2}{A}\right)+\frac{A}{\rho}\frac{\partial P}{\partial x}=-\frac{2\pi vr}{\delta}\frac{q}{A}. \tag{3}$$

The state equation in the arteries is written as,

$$P(x,t)-P_0=\frac{4}{3}\frac{Eh}{r_0}\left(1-\sqrt{\frac{A_0}{A}}\right). \tag{4}$$

The state equation in microcirculation and veins may be expressed as [17],

$$p - p_0 = k_p \left[1 - \left(\frac{A}{A_0} \right)^{-3/2} \right], \tag{5}$$

where k_p is the coefficient proportional to the bending stiffness of the tube wall. We assumed k_p to be constant in all the microcirculation vessels and veins. The value of k_p is taken as 0.5×10^6 Pa. The relationship between the Young's modulus, vessel radius, and wall thickness is expressed empirically, such as,

$$\frac{Eh}{r_0} = k_1 \exp(k_2 r_0) + k_3, \tag{6}$$

where $k_1 = 2.00 \times 10^6$ kg/s^2 m, $k_2 = -2.253 \times 10^3$ m^{-1}, and $k_3 = 8.65 \times 10^4$ kg/s^2 m.

The momentum equation can be expressed as a function of q and A by substituting the state Eq. (4) into Eq. (3) such that,

$$\frac{\partial q}{\partial t} + \frac{\partial}{\partial x}\left(\frac{q^2}{A} + B \right) = -\frac{2\sqrt{\pi} v}{\delta} \frac{q}{\sqrt{A}} + C. \tag{7}$$

For the blood flow in the arteries, parameters B and C can be written as,

$$\begin{aligned} B &= \sqrt{\pi A} \frac{1}{\rho} \frac{4}{3} Eh, \\ C &= \sqrt{\pi A} \frac{8}{3} \frac{1}{\rho} \frac{\partial}{\partial x}(Eh) - \frac{4}{3} \frac{A}{\rho} \frac{\partial}{\partial x}\left(\frac{Eh}{r_0} \right). \end{aligned} \tag{8}$$

For the blood flow in microcirculation and veins, they are expressed as,

$$\begin{aligned} B &= -\frac{3}{\rho} k_p \sqrt{\frac{A_0^3}{A}}, \\ C &= 0. \end{aligned} \tag{9}$$

Note that the friction term for the equivalent tube has the following form:

$$F = \frac{2\sqrt{\pi} v}{\delta} \frac{q}{\sqrt{S/N}}, \tag{10}$$

where S is the total cross-sectional area of the equivalent tube, and N is the total number of vessels.

The energy equation for the elastic vessel is derived based on Keller and Seiler's analytical method [10,11]. As shown in Fig. 2, the energy balance equation for the arterial element may be written as,

$$\begin{aligned} \frac{\partial(\rho_b A c_b T_b)}{\partial t} = &-\frac{\partial(\rho_b A u c_b T_b)}{\partial x} - \omega \rho_b c_b A T_b \\ &- h_{ves} A_s (T_b - T_{tmn}). \end{aligned} \tag{11}$$

Since the density and specific heat are assumed to be constant, and the blood flow rate can be expressed as $q = Au$, Eq. (10) can thus be rewritten in the following non-conservative form, as,

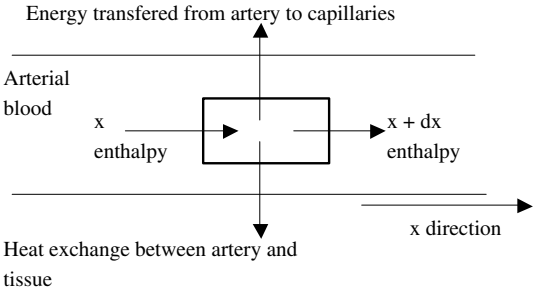

Fig. 2. A schematic view of heat exchange between an artery element and the surroundings.

$$\frac{\partial T_b}{\partial t} + \frac{q}{A} \frac{\partial T_b}{\partial x} = -\omega T_b - \frac{h_{ves} A_s}{\rho_b c_b A} (T_b - T_{tmn}). \tag{12}$$

Note that, unlike in Keller and Seiler's model, the cross-sectional area varies with time and space. Eq. (12) reveals that the energy change in unit time within unit distance is equal to the energy transferred from the artery to the tissues and capillaries. When Eq. (12) is used to compute the blood temperature in capillaries and veins, the first term on the right hand side becomes 0 and ωT_b.

With respect to the mean tissue temperatures T_{tmn}, here, we assumed that the mean tissue temperature throughout the upper limb, except the part of the finger remained constant at 35 °C. The tissue temperature in the finger was computed from Pennes' bioheat equation [18,19], which was written as,

$$\begin{aligned} \rho_t c_t \frac{\partial T_t}{\partial t} = &\frac{1}{r} \frac{\partial}{\partial r}\left(r \lambda_r \frac{\partial T_t}{\partial r} \right) + \frac{1}{r} \frac{\partial}{\partial \theta}\left(\frac{\lambda_\theta}{r} \frac{\partial T_t}{\partial \theta} \right) + q_{met} \\ &+ \omega \rho_b c_b (T_b - T_t). \end{aligned} \tag{13}$$

Hence, by coupling the blood-flow model with the thermal model of solid tissues, the arterial, venuous, capillary, and mean tissue temperature can be obtained. Fig. 3 shows the method of transferring data between

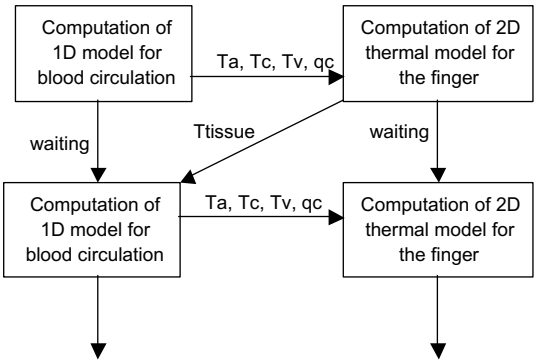

Fig. 3. The coupling method for the blood circulation and thermal models.

the blood circulation model and the thermal model. Initially, the blood circulation model provides the blood flow rate of the capillaries, as well as the arterial, venuous, and capillary temperature to the thermal model. Then, the averaged tissue temperature, which is needed in the blood circulation model, is specified by the thermal model. These steps are repeated until the steady state is attained.

4. Numerical method

The flow rate at an inlet to the ascending aorta is specified in the form of a physiological volumetric flow rate, which is expressed as [20,21],

$$q_{\text{in}} = q_{\max}(0.251 + 0.290(\cos\Phi + 0.97\cos 2\Phi + 0.47\cos 3\Phi + 0.14\cos 4\Phi))$$
$$\Phi = \psi t - \sqrt{\frac{\psi}{\pi}}. \tag{14}$$

The maximum flow rate $q_{\max}$ is defined as in Ref. [6]. The output pressure at the superior vena cava is taken to be constant and assumed to be 5 mm Hg (660 Pa). As the flow, pressure, and temperature are continuous at the bifurcations of the blood vessels, the internal boundary conditions at the bifurcation can be expressed as,

$$\begin{aligned} q_{\text{p}} &= q_{\text{d1}} + q_{\text{d2}}, \\ p_{\text{p}} &= p_{\text{d1}} = p_{\text{d2}}, \\ T_{\text{p}} &= T_{\text{d1}} = T_{\text{d2}}. \end{aligned} \tag{15}$$

With respect to the junction between two equivalent tubes, the boundary conditions are given as,

$$q_{\text{w}} = q_{\text{e}}, \quad p_{\text{w}} = p_{\text{e}}, \quad T_{\text{w}} = T_{\text{e}}. \tag{16}$$

Inflow blood temperature at the ascending aorta is assumed to be 37 °C.

Eqs. (2) and (7) are transformed into an algebraic form using the two-step Lax-Wendroff method. The differencing equation has second-order accuracy in space and time.

Firstly, the flow rate q and cross-sectional area A at the time $n + 1/2$ are computed such as,

$$A_j^{n+1/2} = \frac{1}{2}\left(A_{j+1/2}^{n+1/2} + A_{j-1/2}^{n+1/2}\right) - \frac{\Delta t}{2\Delta x}\left(q_{j+1/2}^{n} - q_{j-1/2}^{n}\right), \tag{17}$$

$$q_j^{n+1/2} = \frac{1}{2}\left(q_{j+1/2}^{n} + q_{j-1/2}^{n}\right) - \frac{\Delta t}{2\Delta x}\left(G_{j+1/2}^{n} - G_{j-1/2}^{n}\right) + \frac{\Delta t}{2}\frac{1}{2}\left(G_{F_{j+1/2}}^{n} + G_{F_{j-1/2}}^{n}\right), \tag{18}$$

where

$$j = i + 1/2 \text{ or } i - 1/2, \quad G = q^2/A + B, \quad G_F = -\frac{2\sqrt{\pi}v}{\delta}\frac{q}{\sqrt{A}} + C. \tag{19}$$

Secondly, the flow rate and the cross-sectional area at time $n + 1$ are computed as,

$$A_i^{n+1} = A_i^{n} - \frac{\Delta t}{\Delta x}\left(q_{i+1/2}^{n+1/2} - q_{i-1/2}^{n+1/2}\right), \tag{20}$$

$$q_i^{n+1} = q_i^{n} - \frac{\Delta t}{\Delta x}\left(G_{i+1/2}^{n+1/2} - G_{i-1/2}^{n+1/2}\right) + \frac{\Delta t}{2}\left(G_{F_{i+1/2}}^{n+1/2} + G_{F_{i-1/2}}^{n+1/2}\right). \tag{21}$$

The cross-sectional area at the time $n + 1/2$ and $n + 1$ for the inlet can be extrapolated using Eqs. (17) and (20).

Solutions of the flow rates and the cross-sectional areas for the outlet and the internal joint points are not as direct as those at inside points, because the q and A are explicitly unknown. With respect to the flow rates and cross-sectional areas at the bifurcations, the discrete equations of the continuity equation at the point $m - 1/2$ for the parent vessel, and at the point $1/2$ for the daughter vessel are used [7].

$$\frac{\frac{A_{m-1}^{n+1} + A_m^{n+1}}{2} - \frac{A_{m-1}^{n} + A_m^{n}}{2}}{\Delta t} + \frac{q_m^{n+1} - q_{m-1}^{n+1}}{\Delta x} = 0, \tag{22}$$

$$\frac{\frac{A_0^{n+1} + A_1^{n+1}}{2} - \frac{A_0^{n} + A_1^{n}}{2}}{\Delta t} + \frac{q_0^{n+1} - q_1^{n+1}}{\Delta x} = 0. \tag{23}$$

Substituting Eqs. (22) and (23) into the boundary conditions (Eqs. (15) and (16)) results in a set of nonlinear equations which may be solved using Newton's method. A similar method may also be used in computing the flow rates and the cross-sectional areas at other joint points.

The blood temperature can be obtained by the discretization of Eq. (12), in which the upwind scheme is introduced for the convective term, as:

$$T_{b_i}^{n+1} = T_{b_i}^{n} - \frac{\Delta t}{\Delta x}\frac{q_i^n}{A_i^n}\left(T_{b_k}^{n} - T_{b_{k-1}}^{n}\right) - \Delta t\omega T_{b_i}^{n} - \frac{\Delta t}{\rho_{\text{b}} c_{\text{b}}}\frac{h_{\text{ves}} A_{s_i}^{n}}{A_i^{n}}\left(T_{b_i}^{n} - T_{\text{tmn}}\right), \tag{24}$$

where

$$k = \begin{cases} i & \text{if } q/A > 0, \\ i + 1 & \text{if } q/A < 0. \end{cases} \tag{25}$$

With regard to the temperature at a new step at the last point of a single vessel, when the reverse flow appears, we assume that the temperature at a ghost point $m + 1$ is equal to the temperature at point m, such that,

$$T_{b_m}^{n+1} = T_{b_m}^{n} - \Delta t \omega T_{b_m}^{n} - \frac{\Delta t}{\rho_b c_b} \frac{h_{ves} A_{s_m}^{n}}{A_m^{n}} \left(T_{b_m}^{n} - T_{tmn}\right) \quad \text{if } q/A < 0. \tag{26}$$

The stability criterion for the linearized equations is,

$$\Delta t \leqslant \frac{\Delta x}{c}, \tag{27}$$

where c is the wave propagation velocity defined as [6],

$$c = \left| \frac{q}{A} \pm \sqrt{\frac{A}{\rho} \frac{\partial p}{\partial A}} \right|. \tag{28}$$

Accordingly, Δx is taken as larger than 1×10^{-3} m, and Δt is taken as less than 1×10^{-5} s in the present model. The flow chart of the computation is depicted in Fig. 4.

5. Results and discussion

The computational parameters used in the present numerical analysis are listed in Table 3. Computed results for a normal case are illustrated in Figs. 5–7. Fig. 5 shows the pressure distributions in four different blood vessels. It can be seen that the largest pressure drop occurs between the terminal arteries and the capillaries, and there is only a slight pressure drop between the aorta and the terminal arteries. These results are in agreement with the normal physiological process in the human circulation system. The computed mean pressures for the aorta, arteries, capillaries, and veins are 112 mm Hg (No. 1), 75 mm Hg (No. 10), 21 mm Hg (No. 26), and 10 mm Hg (No. 30) respectively, which are very close to the available data given in Ref. [14]. (The mean

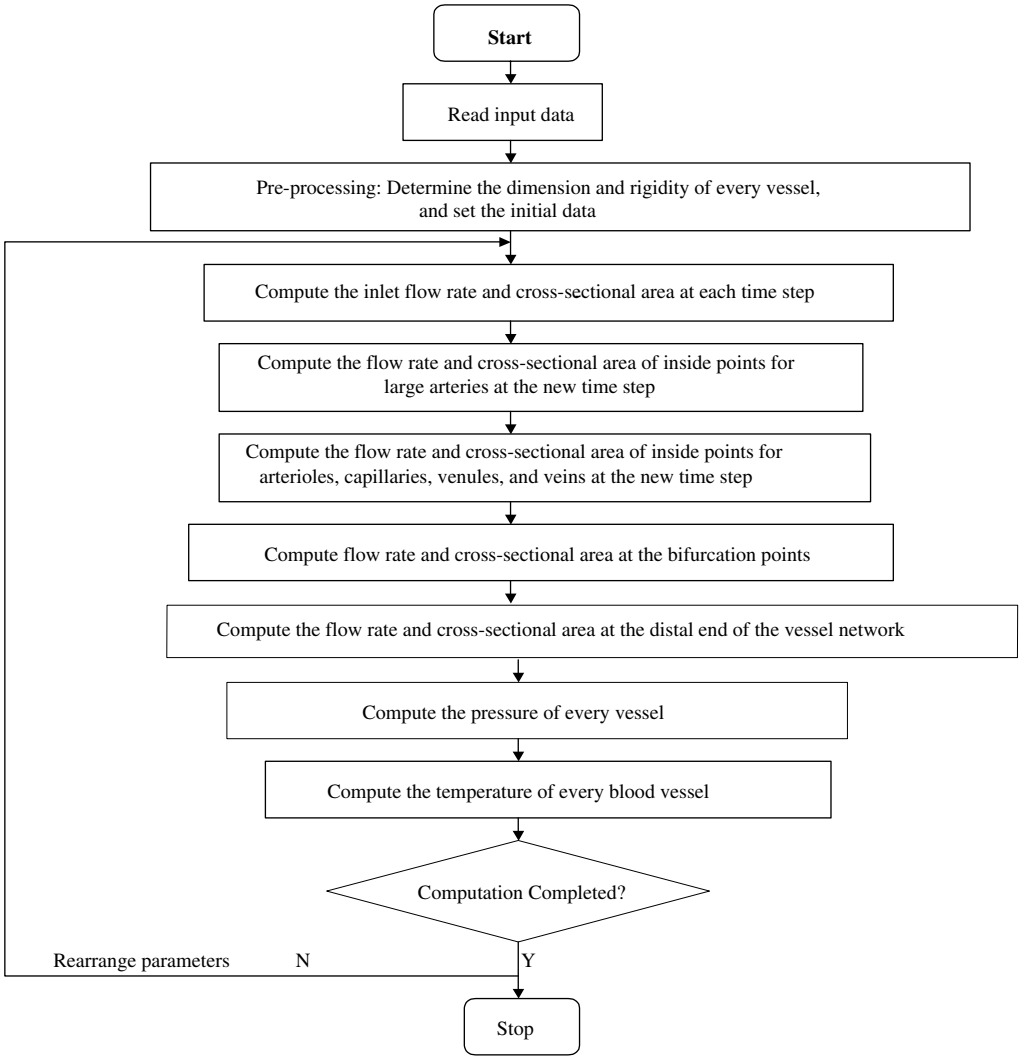

Fig. 4. Flow chart of the basic computations.

Table 3
Parameters used in the numerical analysis

v (m^2/s)	4.0×10^{-6}
ρ_b (kg/m^3)	993
c_b (J kg/K)	3300
h_{art} (W/m^2 K)	1800
ω (m^3 blood/s/m^3 tissue)	0.0005–0.0008

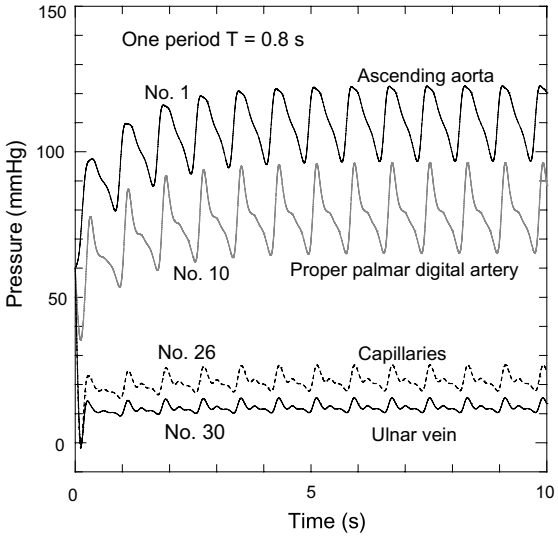

Fig. 5. Computed pressure signals in different blood vessels.

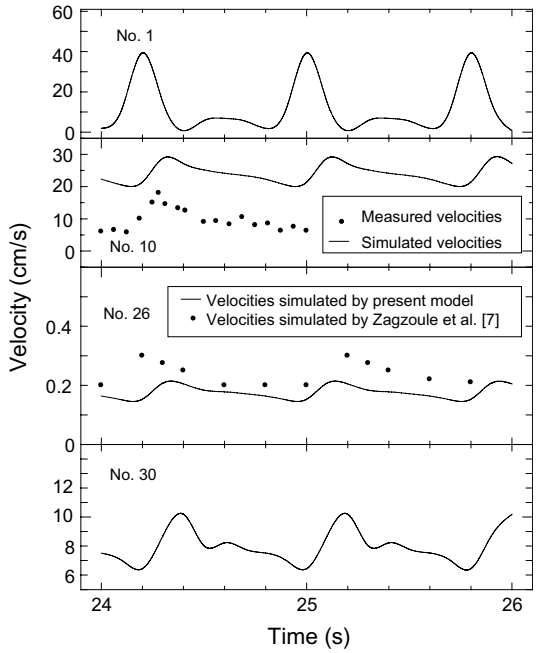

Fig. 6. Computed temporal blood velocities in the same blood vessels as those in Fig. 5.

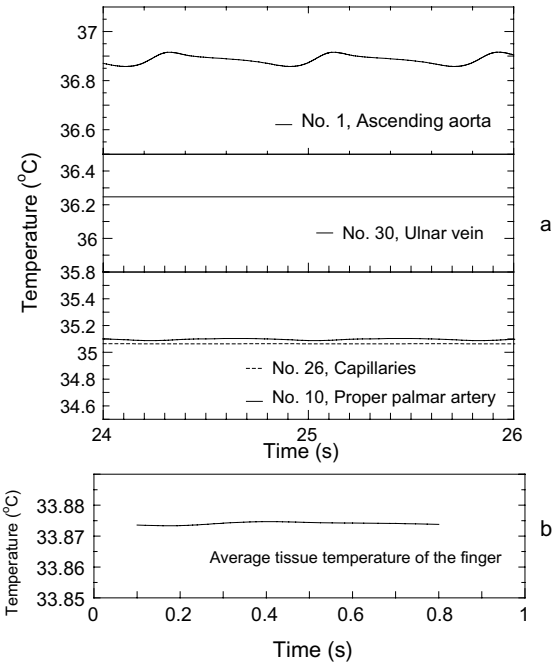

Fig. 7. Predicted temporal blood temperatures in the same blood vessels as those in Fig. 5 (a) and predicted average tissue temperature (b).

pressures in the aorta, arteries, capillaries, and veins are 100, 90, 30–20, and 15–10 mmHg respectively.)

Fig. 6 shows the computed blood velocities in four different vessels (Nos. 1, 10, 26 and 30). From the ascending aorta to the capillaries, the pulsatile feature tends to be damped due to viscous friction, but is gradually enhanced from the capillaries to the returning veins. The blood velocities in the proper palmar artery, measured by the Bi-directional Doppler DVM-4300 (HADECO) are plotted for the comparison with the predicted velocities in vessel No. 10. It is observed that the computed results are larger than the measurements. This is due to the fact that we only considered the main bifurcations in the peripheral region; this resulted in higher flow rates in that peripheral region. There is little available data on blood velocity in capillaries. We plotted the computational data on cerebral capillaries obtained by Zagzoule and Marc-Vergnes [7]. Compared to their data, the velocities computed by the present model are lower. However, the computed mean velocity (0.17 cm/s) is higher than the data provided in Ref. [14] (< 0.1 cm/s). The computed average velocities from the venules to the vena cava are between 0.5–13 cm/s, which is a reasonable range compared to the data in Ref. [14] (0.3–30 cm/s).

Correspondingly, the temporal variations of the temperature in the steady state for the same vessels are shown in Fig. 7. In the arteries, the temperature varies

with the pulsation of the blood flow corresponding to the heart beat period. With a decrease in the arterial diameters, there is a decrease in the temperature pulsation varying approximately from 0.06 °C in the ascending aorta, to 0.01 °C in the proper palmar artery. The temperature pulsating is not observed in the capillaries and veins. Fig. 7b shows the average tissue temperature of the finger, computed by coupling the thermal model [19]. An extremely small pulsating variation can be observed in the average tissue temperature of the finger.

Fig. 8 shows the average blood temperature (a) and blood flow rate (b, c) distribution in the circulation system of the human upper limb. The horizontal axis depicts the number of vessels shown in Fig. 1. The statistical data on the blood flow temperature [22] are also plotted. We can see that the computed average blood temperature shows the same tendency as the statistical data. It is noted that the temperatures in the peripheral artery (No. 10) and veins (No. 27, 30) have larger deviations compared with the statistical data. It is considered that this is due to the effect of the perfusion rate of blood flow, ω. It is not easy to determine the local perfusion rate of blood flow. In this model, for larger arteries, veins, and capillaries (Nos. 1–5, 31–34, and 26), the perfusion rates are set as 0 (there is no blood flow perfused to/from capillaries), and a constant perfusion rate is considered for the other blood vessels. Thus, the blood perfusion rate can significantly affect the temperature in these vessels.

The average blood flow rates in different vessels are plotted in Fig. 8b and c. Fig. 8c shows the blood flow rates in peripheral vessels. It is observed that the blood temperatures are closely related to the variations in the blood flow rate, especially in the peripheral region.

In the present model, two parameters are introduced to represent vessel wall stiffness. The term Eh/r_0 expresses the stiffness of the tube wall in the arteries, and k_p represents the stiffness of the tube wall in the arterioles, capillaries, and veins. Fig. 9a and b show the temperature profile and pressure distribution when the bending stiffness of the arterial wall varies. It can be seen that the diastolic arterial pressure tends to increase, but the systolic arterial pressure decreases as the wall of the arterial vessel becomes stiffer. However, the temperature variation is minimal, and the arterial and venous temperatures are only slightly higher than those in a normal physiological situation.

The influence of blood viscosity on pressure and temperature was investigated. In the present model, we assumed that the fluid kinematic viscosity is constant in all the vessels. This approximation may be reasonable with respect to most blood vessels. The temperature and pressure profiles with varying blood viscosity are plotted in Fig. 10a and b. The results show that, as viscosity increases, the highest and lowest pressure also increases significantly, and the blood temperature in the peripheral arteries decreases accordingly.

Smoking is considered to increase blood viscosity [23]. The predicted tendency of the pressure and blood flow is in agreement with experimental studies carried out on the influence of smoking [2].

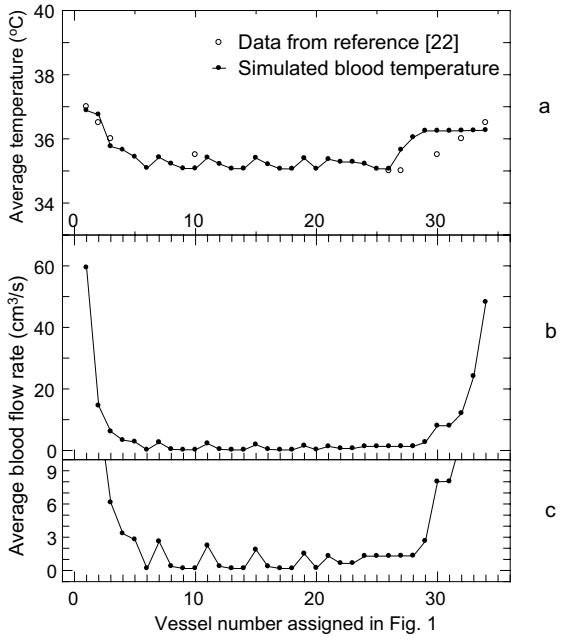

Fig. 8. Average blood temperature distribution (a) and blood flow rate distribution (b, c) in the circulation system of the human upper limb.

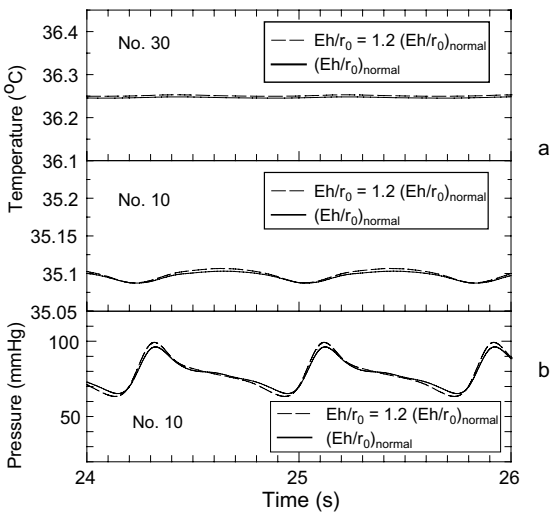

Fig. 9. Temperature (a) and pressure (b) variations for different wall stiffness of blood vessels.

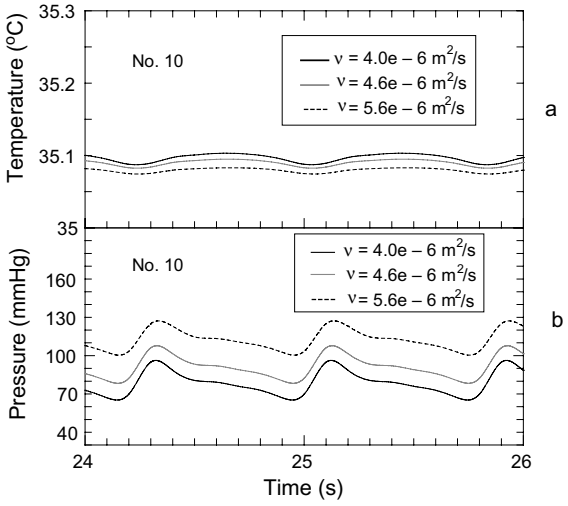

Fig. 10. Temperature (a) and pressure (b) variations for different blood viscosity.

Although the present model cannot yet predict the effects of wall stiffness and viscosity with certainty, the investigation provides a good beginning.

6. Concluding remarks

A one-dimensional thermo-fluid model of blood circulation in the upper limb of humans has been developed. The hemodynamic model of arteries, capillaries, and veins is developed, based on the structured-tree arterial model [6]. In the energy equation, not only the blood flow rate, but also the cross-sectional area of the blood vessel is included. Hence, the present model can predict the influence of the blood flow rate, and the blood pressure as well as that of the cross-sectional area on the blood temperature.

The computed results of blood flow in four different vessels obtained using the statistical morphological data, are presented and discussed. The comparison with the limited measurements and the available data in the references shows that the computed results are, basically, in agreement with this data. The influence of the stiffness of the vessel wall as well as that of the viscosity of the blood is discussed. With the present model, we have conducted a series of experimental and theoretical studies on the relationship between the blood flow rate, the blood pressure, and the blood temperature.

References

[1] P. Nketia, S. Reisman, The relationship between thermoregulatory and haemodynamic responses of the skin to relaxation and stress, in: Proceedings of the IEEE 23rd Northeast Bioengineering Conference, IEEE, New York, NY, USA, 1997, pp. 27–28.

[2] S. Bornmyr, H. Svensson, Thermography and laser-Doppler flowmetry for monitoring changes in finger skin blood flow upon cigarette smoking, Clin. Physiol. 11 (1991) 135–141.

[3] J.P. Cooke, M.A. Creaker, P.H. Osmundson, J.T. Shepherd, Sex differences in control of cutaneous blood flow, Circulation 82 (1990) 1607–1615.

[4] W.L. Kenney, G. Havenith, Thermal physiology of elderly and handicapped, heat stress and age: skin blood flow and body temperature, J. Therm. Biol. 18 (1993) 341–343.

[5] T. Kitawaki, M. Shimizu, R. Himeno, H. Liu, One-dimensional numerical simulation of blood flow in a visco-elastic tube with consideration of unsteady viscous resistance and visco-elasticity of the tube blood flow in multi branched arteries, Trans. JSME J. Ser. A 69 (677) (2003) 1–8.

[6] M.S. Olufsen, C.S. Peskin, W.Y. Kim, E.R. Pedersen, A. Nadim, J. Larsen, Numerical simulation and experimental validation of blood flow in arteries with structured-tree outflow conditions, Ann. Biomed. Eng. 28 (2000) 1281–1299.

[7] M. Zagzoule, J. Marc-Vergnes, A global mathematical model of the cerebral circulation in man, J. Biomech. 19 (12) (1986) 1015–1022.

[8] C.W. Li, H.D. Cheng, A nonlinear fluid model for pulmonary blood circulation, J. Biomech. 26 (6) (1993) 653–664.

[9] C. Sheng, S.N. Sarwal, K.C. Watts, A.E. Marble, Computational simulation of blood flow in human systemic circulation incorporating an external force field, Med. Biol. Eng. Comput. 33 (1995) 8–17.

[10] K.H. Keller, L. Seiler, An analysis of peripheral heat transfer in man, J. Appl. Physiol. 30 (1971) 779–786.

[11] C.K. Charny, Mathematical models of bioheat transfer, in: Y.I. Cho (Ed.), Bioengineering Heat Transfer; Advances in Heat Transfer, Academic Press, 1992, pp. 19–152.

[12] O.I. Craciunescu, S.T. Clegg, Pulsatile blood flow effects on temperature distribution and heat transfer in rigid vessels, Trans. ASME, J. Biomech. Eng. 123 (2001) 500–505.

[13] Y. He, M. Shirazaki, R. Himeno, A finite element model for determining the effects of blood flow on the finger temperature distribution, in: Proceedings of the 6th ASME-JSME Thermal Engineering Joint Conference, Hawaii, 2003, TED-AJ03-166.

[14] S.A. Berger, Physiological fluid mechanics, in: S.A. Berger, W. Goldsmith, E.R. Lewis (Eds.), Introduction to Bioengineering, Oxford University Press, 2000, pp. 133–201.

[15] W. Kahle, H. Leonhardt, W. Platzer, Taschenatlas der Anatomie (in Japanese, translated by J. Ochi), Bunkodo, 2000, pp.166–252.

[16] N. Sterglopuls, D.F. Young, T.R. Rogge, Computer simulation of arterial flow with applications to arterial and aortic stenoses, J. Biomech. 25 (1992) 1477–1488.

[17] A.H. Shapiro, Steady flow in collapsible tubes, Trans. ASME, J. Biomech. Eng. 99 (1977) 126–147.

[18] H.H. Pennes, Analysis of tissue and arterialblood temperatures in the resting human forearm, J. Appl. Physiol. 1 (2) (1948) 93–122.

[19] Y. He, T. Kawamura, R. Himeno, A two-dimensional thermal model for determining cold-stressed effects on a human finger (Japanese), in: Proceedings of 38th National Heat Transfer Symposium of Japan, 2001, pp. 209–210.
[20] H. Liu, T. Yamaguchi, Waveform dependence of pulsatile flow in a stenosed channel, Trans. ASME J. Biomech. Eng. 123 (2001) 88–96.
[21] D.A. McDonald, Blood Flow in Arteries, second ed., Arnold, London, 1974.
[22] M. Iriki, The Physiology to understand human skin temperature, in: I. Fujimasa (Ed.), Physiological Function Imaging Thermography, Shujunsha, 1988, pp.13–19 (in Japanese).
[23] M. Imaizumi, Y. Isaka, K. Ashida, Y. Abe, Smoking and cerebral blood circulation, Smoking Research Foundation http://www.srf.or.jp/histoly/papers/06.html (in Japanese).